


RESEARCH ARTICLE

Open Access



Scalability of future climate changes across Japan examined with large-ensemble simulations at + 1.5 K, +2 K, and + 4 K global warming levels

Masaya Nosaka^{1*} , Masayoshi Ishii¹, Hideo Shioyama², Ryo Mizuta¹, Akihiko Murata¹, Hiroaki Kawase¹ and Hidetaka Sasaki¹

Abstract

Large-ensemble climate experiments were performed to simulate future climates for a + 1.5 K rise in the global mean surface air temperatures relative to preindustrial levels as a subset of the database for Policy Decision making for future climate change (d4PDF), using the Non-Hydrostatic Regional Climate Model (NHRCM) with 20 km grid spacing. Along with present climate, + 2 K and + 4 K experimental outputs from the d4PDF already available, we investigated responses of surface air temperature (SAT) and precipitation on regional scales over Japan to global warming. The reproducibility of the present climate experiment is satisfactory to investigate future changes in the Japanese climate, and dynamical downscaling from the global to the regional climate states improves the frequency of heavy daily precipitation. In the future, SAT over Japan rises linearly with and faster than the global mean SAT. The meridional contrast of SAT rises becomes more pronounced as global warming progresses. Winter precipitation decreases/increases linearly in the western/eastern Japan, reflected by weakening of future winter monsoons. Annual maximum daily precipitation (R1d) shows a closely linear increase with the global SAT rise, but annual precipitation is mostly unchanged. The global mean SAT change from + 1.5 to + 2 K enhances R1d by 2.7% over the Japanese Islands, although the increase of R1d varies by regions. The increase in R1d is 5% in northern Japan, where the SAT increases are greater than those in other regions.

Keywords: Climate change, Regional climate model, Large-ensemble climate experiments, Paris Agreement, Surface air temperature, Precipitation

Introduction

The Meteorological Research Institute has been developing a non-hydrostatic regional climate model (NHRCM, Sasaki et al. 2008) to predict the future climate for Japan based on an operational non-hydrostatic model from the Japan Meteorological Agency. We performed high-resolution climate simulations using 5 km grid spacing and using 2 km grid spacing NHRCMs nested from the

global model with 20 km grid spacing (Mizuta et al. 2012; Murata et al. 2017). Increasing the resolution of the NHRCM improves the representation of the terrain and leads to the elucidation of detailed physical processes. Murata et al. (2017) showed that the NHRCM better represents the extremes of surface air temperature (SAT) and precipitation by increasing the horizontal resolution from 5 to 2 km. However, since the high-resolution model integration requires sizable computational resources, it is not easy to conduct large-ensemble simulations for estimations of the uncertainties in the model-simulated variables.

* Correspondence: snosaka@mri-jma.go.jp

¹Meteorological Research Institute, 1-1 Nagamine, Tsukuba, Ibaraki 305-0052, Japan

Full list of author information is available at the end of the article



© The Author(s). 2020 **Open Access** This article is licensed under a Creative Commons Attribution 4.0 International License, which permits use, sharing, adaptation, distribution and reproduction in any medium or format, as long as you give appropriate credit to the original author(s) and the source, provide a link to the Creative Commons licence, and indicate if changes were made. The images or other third party material in this article are included in the article's Creative Commons licence, unless indicated otherwise in a credit line to the material. If material is not included in the article's Creative Commons licence and your intended use is not permitted by statutory regulation or exceeds the permitted use, you will need to obtain permission directly from the copyright holder. To view a copy of this licence, visit <http://creativecommons.org/licenses/by/4.0/>.

Mizuta et al. (2017) created a climate simulation dataset, called the database for Policy Decision making for future climate change (d4PDF), using the Meteorological Research Institute atmospheric general circulation model (MRI-AGCM, Mizuta et al. 2012) with 60 km grid spacing and the NHRCM with 20 km grid spacing. The database contains the outputs of large-ensemble experiments over a 5000 year span under present and future climate conditions; in the latter, the global average SAT is 4 K higher relative to preindustrial levels. Fujita et al. (2019) created a dataset for + 2 K conditions as a sub-dataset of the d4PDF for risk assessments of extreme weather events based on the 2 K goal of the Paris Agreement. The resolution of the model used for the d4PDF is coarse compared to the experiments using 2 km or 5 km grid spacings, but many model-simulated samples of infrequent phenomena are available thanks to large-ensemble simulations. Kawase et al. (2016) showed that rare and strong snowfall amounts in mountainous areas became stronger under a + 4 K climate scenario than under the present climate. Fujita et al. (2019) investigated the future changes of the relationship between extreme hourly precipitation events and daily mean SATs in Japan, and found that hourly precipitation will become stronger for higher-SAT days and slightly weaker for lower-SAT days in the future.

The Paris Agreement aims to pursue efforts to limit the SAT rise to + 1.5 K, and to at least keep the global temperature increase below + 2 K compared to preindustrial levels. Researchers have been investigating the differences of changes in extreme events and impacts on human society and on ecosystems between the + 1.5 and + 2 K warming cases (Masson-Delmotte et al. 2018). In a research project, the HAPPI (half a degree additional warming, projections, prognosis, and impacts) multimodel experiments (Mitchell et al. 2016; Mitchell et al. 2017) provided an assessment framework and a simulation dataset for climates at the + 1.5 K and + 2 K levels. Liu et al. (2018) showed that a moderation of drought risks appears between + 1.5 and + 2 K levels. Lee et al. (2018) indicated that warming by more than half a degree brings more intense and more frequent precipitation events to the Asian monsoon region. Shiogama et al. (2019) suggested that regions with relatively large increases of extreme hot days, heavy rainfall, high streamflow and labor capacity reductions related to heat stress coincide with those countries that are characterized by low CO₂ emissions, low income, and high vulnerability. Limiting global warming to 1.5 K, compared to 2 K, lowers these inequalities.

Most studies of the + 1.5 K climate simulation have used global models, but von Trentini et al. (2019) and Leduc et al. (2019) used regional climate models for the European and North American domains, respectively.

However, there was no regional climate dataset that represented spatially detailed climate states around Japan under the + 1.5 K climate scenario.

The purpose of this study is to investigate the regional characteristics of the increase rate of surface air temperature and precipitation using the large ensemble past and future climate simulation assuming + 1.5 K, + 2 K, and + 4 K relative to preindustrial period. For this purpose, over a 1500 year span of ensemble + 1.5 K climate simulations with the NHRCM was performed as a subset of the d4PDF. We discuss the linearity of regional climate states for the present, + 1.5 K, + 2 K, and + 4 K climates, that is, scalability. In addition, we present results which suggest the necessity of additional mitigation measures for the + 2 K climate case rather than for the + 1.5 K climate case.

Methods/Experimental

Experimental design

We used the MRI-AGCM with a 60 km grid spacing (Mizuta et al. 2012) and the NHRCM20 with a 20 km grid spacing (Sasaki et al. 2008). Using the MRI-AGCM outputs as boundary conditions, dynamical downscaling was performed with the NHRCM20. The experimental design followed Mizuta et al. (2017) and Fujita et al. (2019), who conducted large-ensemble experiments under the past climate condition (PAST), + 2 K (d2), and + 4 K (d4) global mean SAT (gSAT) conditions. In this study, we conducted experiments for the + 1.5 K gSAT case relative to preindustrial levels (d1.5).

One hundred simulations of the present climate experiments had already been conducted for the period from 1951 to 2010 (Mizuta et al. 2017), in which the monthly sea surface temperature observations (COBE-SST2, Hirahara et al. 2014) were prescribed. In each simulation, the atmospheric models were perturbed by different initial conditions and by spatio-temporally varying sea surface temperatures (SST) perturbations. The SST perturbations reflect the observational uncertainties.

In the + 1.5 K experiment, we prescribed the SSTs that represent future SST patterns (Δ SSTs) obtained from six models of the Coupled Model Intercomparison Project Phase 5 (CMIP5) plus the detrended COBE-SST2. The future SST patterns are the differences between the averages for 1991–2010 in the historical experiments and those for 2020–2039 in the Representative Concentration Pathway 8.5 (RCP8.5) scenario experiments. To force the gSATs of the + 1.5 K experiment with MRI-AGCM to become + 1.5 K, each Δ SST was multiplied by a scaling factor (Table 1; Shiogama et al. 2010) which was estimated from the gSAT changes in the CMIP5 experiments (Mizuta et al. 2017). For the greenhouse gas and aerosol concentrations, the values for 2030 in the RCP8.5 scenario were used. Nine ensemble simulations

Table 1 Scaling factors for future SST trend patterns obtained from CMIP5 RCP8.5 runs by six models

Model	Scaling factor
CCSM4	1.05828
GFDL-CM3	0.638859
HadGEM2-AO	1.17874
MIROC5	1.01876
MPI-ESM-MR	1.09218
MRI-CGCM3	1.22361

The six climate models are CCSM4, GFDL-CM3, HadGEM2-AO, MIROC5, MPI-ESM-MR, and MRI-CGCM. See the “Abbreviations” section for their full forms

starting from different initial conditions were performed with the aforementioned future SSTs added to the SST perturbations. The integration period of the + 1.5K climate simulations was 29 years, in which the interannual variations of the SSTs are those from 1982 to 2010. The total number of ensembles is 1566 years. Unless otherwise noted, 1450 years are used for analysis of the PAST and 1566 years are used for analysis of the future climate experiments.

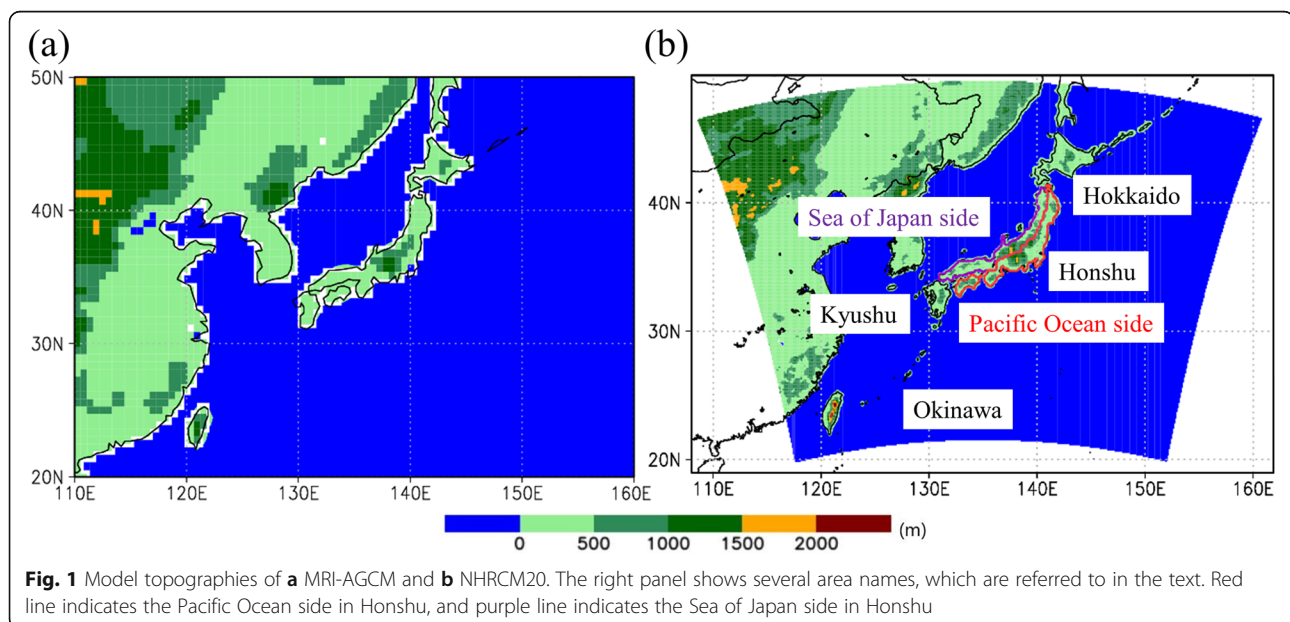
Results and Discussion

Reproducibility of the present climate over the Japanese region

Dynamical downscaling of the NHRCM improves the expressions of topographic effects and the reproduction of extreme phenomena, and maintains the synoptic fields of the MRI-AGCM. Areas of complex mountainous terrain along the center of Japan are more realistically reproduced by the NHRCM20 than by the MRI-AGCM (Fig. 1). The distributions of the climatological sea-level pressures (SLP) and the SATs simulated by

NHRCM20 under the present climate condition are similar to those of the MRI-AGCM (Fig. 2a–b). The precipitation amounts in the mountainous areas of Honshu and on the Sea of Japan side are greater for the NHRCM than for the AGCM because of the realistic expression of topography in the NHRCM. The frequency of daily precipitation events is more realistic in the NHRCM20 than in the MRI-AGCM (Fig. 2c). The NHRCM20 has a frequency of daily precipitation that is below 300 mm, close to the observations, and it can reproduce strong daily precipitation amounts greater than 500 mm.

Figure 3a–c shows the scatter plots of the simulated and observed daily surface air temperatures (SAT). Here, the Automated Meteorological Data Acquisition System (AMeDAS) is used as the observation data, and the model grid data closest to the AMeDAS stations are used for comparison. The daily mean SATs (Tmean) agree with the observations so that the model-simulated values are located mostly along the identical line. The bias, root mean square difference (RMSD) and correlation coefficient between the model-simulated and observed Tmean values are 0.48, 1.0 K, and 0.98, respectively (Table 2). The annual minimum SATs (Tmin) values are also reproduced well by the NHRCM20, especially at grid points where the temperatures are greater than - 15 °C and are distributed mostly along identical lines. Although the annual maximum SATs (Tmax) are distributed near identical lines, the model-simulated temperatures are generally slightly underestimated and are overestimated at some grid points in those specific areas where the topographic effects are great. The Tmin values of the NHRCM20 are highly biased for observed minimum temperatures below



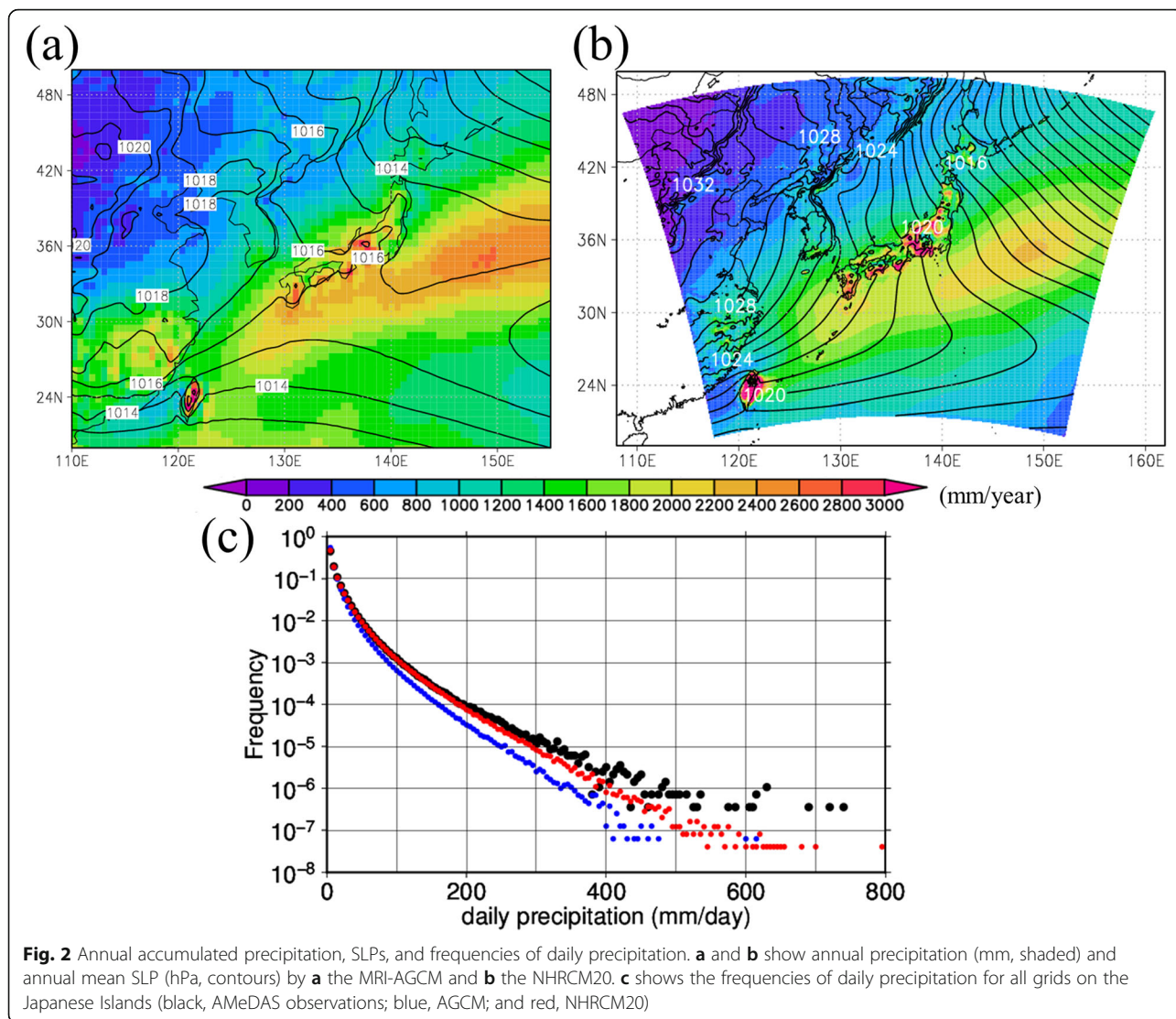


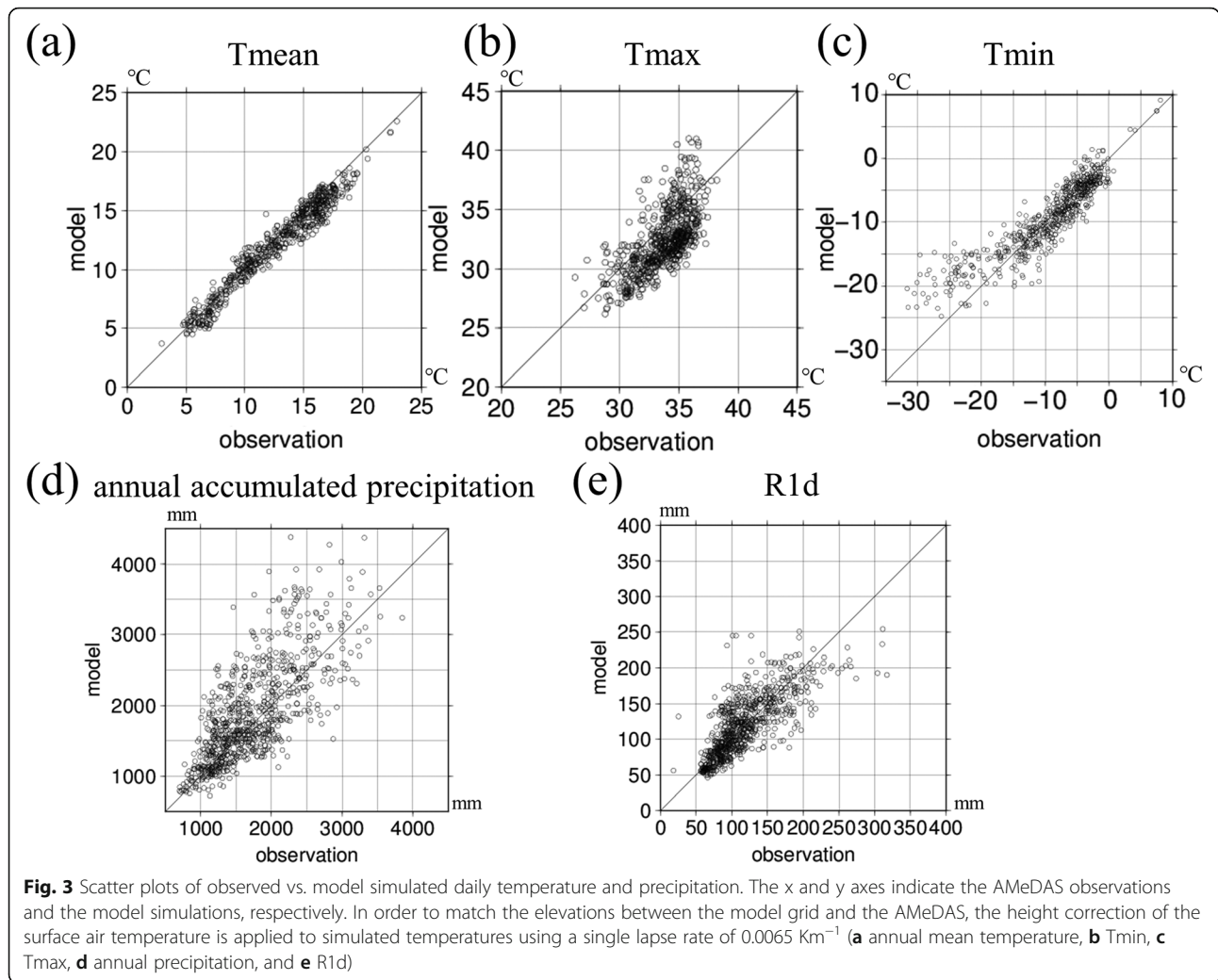
Fig. 2 Annual accumulated precipitation, SLPs, and frequencies of daily precipitation. **a** and **b** show annual precipitation (mm, shaded) and annual mean SLP (hPa, contours) by **a** the MRI-AGCM and **b** the NHRCM20. **c** shows the frequencies of daily precipitation for all grids on the Japanese Islands (black, AMeDAS observations; blue, AGCM; and red, NHRCM20)

- 15 °C. This is due to a “no sea-ice condition” in the Okhotsk Sea during the entire simulation, which is a mistake in all experiments of the d4PDF with the NHRCM20. As a result, the T_{min} values in eastern Hokkaido are overestimated in the simulations. The simulated T_{max} values are biased by - 1.2 K compared to the observations (Fig. 3b and Table 2). This is speculated to be due to the land-cover category definition and the land surface scheme currently adopted in the NHRCM20. This improvement is a future work.

Figure 3d shows a scatter plot of the annual accumulated precipitations. The annual precipitation is reasonably well reproduced by the NHRCM20 with bias of 9%, an RMSD of 28%, and a correlation coefficient of 0.78. The biases are smaller than the standard deviations of the interannual variations for 60% of all stations. Figure 3e shows a scatter plot of the annual maximum daily precipitation (R1d). The annual maximum daily precipitation is well reproduced by the

NHRCM20 with slightly better values for the bias, the RMSD, and the correlation coefficients than those of the annual averages. The biases at 90% of all stations are smaller than the standard deviations of the interannual R1d's.

Murata et al. (2017) conducted present-climate simulations with a 5 km-mesh NHRCM (NHRCM05) and with a 2 km-mesh NHRCM using an urban canopy model (NHRCM02) over a 20 year span. The NHRCM20 shows good performance for the daily scale precipitation and temperatures compared to the NHRCM05 and the NHRCM02, although an increase in the horizontal resolution slightly improves the reproducibility of the SATs and of the precipitation levels due to the effects of topography (Table 2). This result is consistent with that of Takayabu and Hibino 2016. We cannot conduct large-ensemble experiments with high-resolution models due to limitations of computational resources. Note that the lateral boundary conditions of the NHRCM05 and the



NHRCM02 are the MRI-AGCM, with an approximate 20 km horizontal resolution, which are different from that of the NHRCM20 conducted in this study. In this sense, the NHRCM20 has an advantage in performing large-ensemble simulations. Note that a great advantage of the 2 km- and 5 km-resolution NHRCMs is the high reproducibility of sub-daily heavy precipitation events required by the assessment studies (Sasaki et al. 2011).

Future changes in SATs

Figure 4 shows the future changes in the SATs. The north-south contrasts of SAT warming are seen clearly in d2 and d4. The SAT increases in winter are larger than in summer. In winter, the temperature increases are greater in the mountainous areas of Honshu compared to the surrounding plains. Such features are not seen in summer.

Table 2 Biases, RMSDs, and correlation coefficients

Resolution	Bias			RMSE			Correlation coefficient		
	20 km	5 km	2 km	20 km	5 km	2 km	20 km	5 km	2 km
Tmean	0.48 K	- 0.38 K	0.36 K	1.0 K	0.66 K	0.77 K	0.98	0.99	0.99
Tmax	- 1.2 K	- 2.1 K	- 0.31 K	2.5 K	2.3 K	2.0 K	0.69	0.86	0.78
Tmin	0.27 K	- 1.5 K	- 1.1 K	3.1 K	3.4 K	2.9 K	0.91	0.91	0.93
Annual precipitation	9.0%	11%	1.0%	28%	22%	14%	0.75	0.83	0.91
R1d	1.1%	5.6%	7.8%	25%	21%	22%	0.77	0.87	0.89

Tmean, Tmin, Tmax, annual precipitation, and R1d in NHRCM20, NHRCM05, and NHRCM02 are compared to the AMeDAS observations

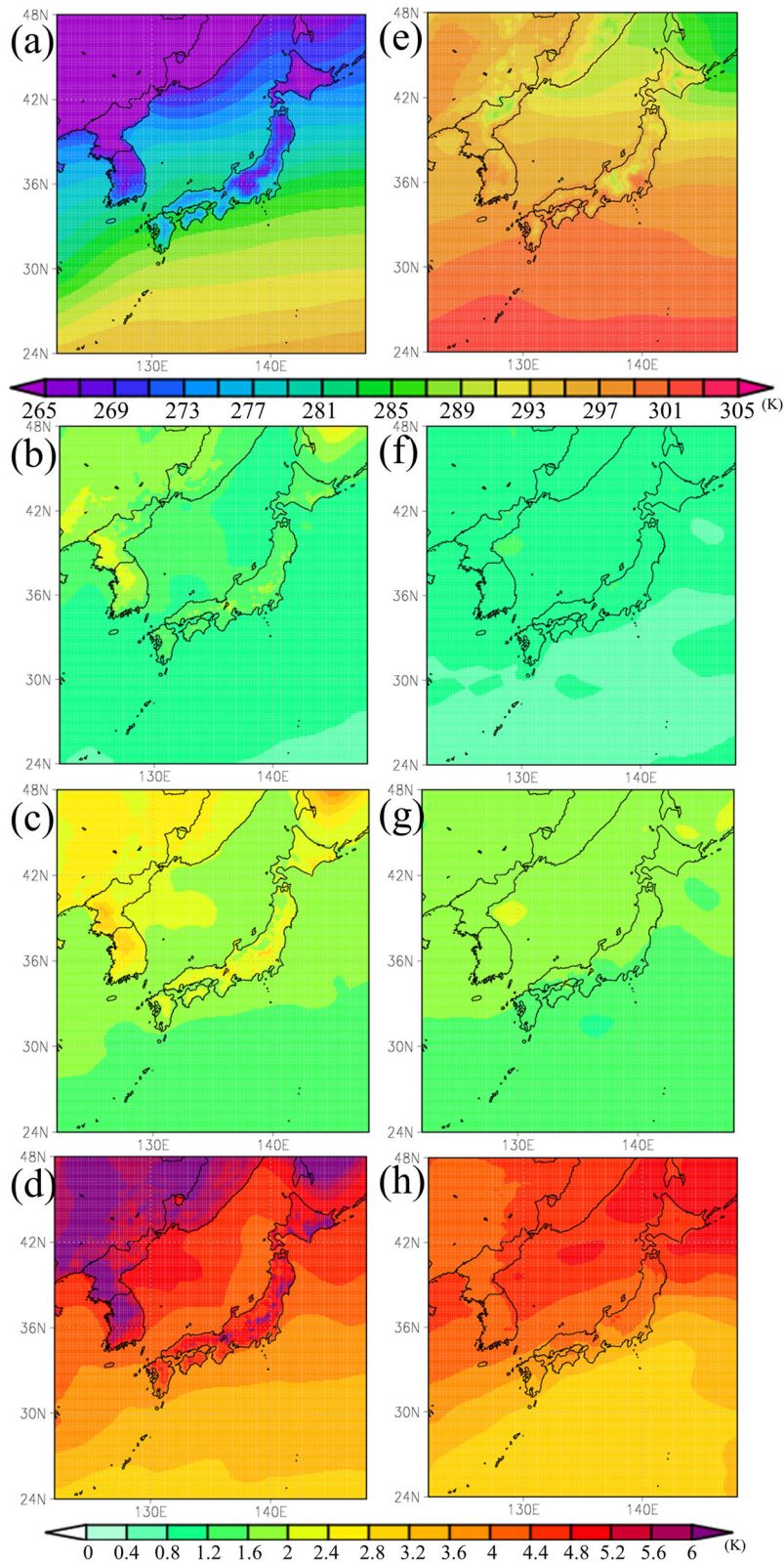


Fig. 4 Seasonal mean SATs and future SAT changes. Seasonal mean SATs (K) of PAST (**a** and **e**) and the future SAT changes of d1.5 (**b** and **f**), d2 (**c** and **g**), and d4 (**d** and **h**). Values for DJF and JJA are shown in the left and right columns, respectively. The mean values are based on 1450 years for PAST and 1566 years for the future climate

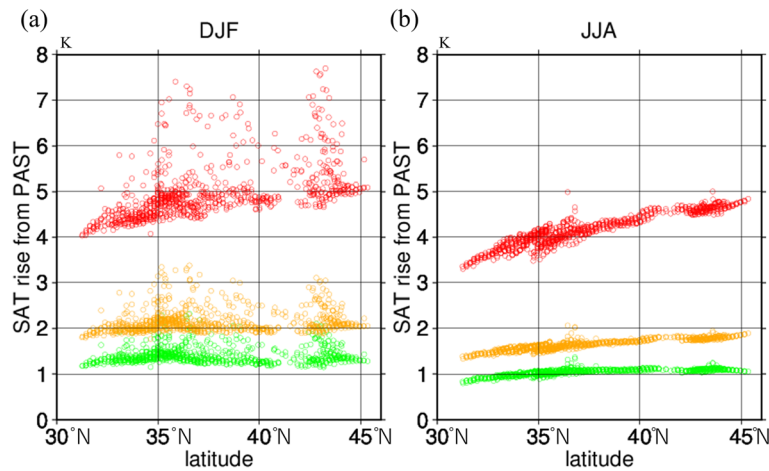


Fig. 5 Scatter plots of increases in seasonal mean SAT relative to the present climate as a function of latitude. **a** DJF and **b** JJA. Values at all land grids on the Japanese Islands were used and were based on 1450 years average for PAST and 1566 years average for the future climate. The green, yellow, and red circles indicate d1.5, d2, and d4, respectively

Figure 5 shows the relationships between latitude and SAT increases. As mentioned above, the distributions of the SAT warming over Japan are caused by the Δ SST distributions (Fig. S1) and the anthropogenic forcing given in the d4PDF experiments (Mizuta et al. 2017). The meridional gradient for d1.5 is generally zero, while greater warming in the northern region is clear in d2 and in d4. As decreases in snow accelerate SAT increases due to snow-albedo feedback (Matsumura and Sato 2011; Scherrer et al. 2012), future SAT increases appear abnormally large in winter for those grid points covered by snow in PAST. In summer, the relationship between latitude and the SAT increases is clear for d2 and d4 with meridional gradients (\pm standard deviations) of $+ 0.029 \pm 0.020 \text{ K}^{-1}$ and $+ 0.089 \pm 0.025 \text{ K}^{-1}$, respectively. The change for d1.5 is $+ 0.013 \pm 0.022 \text{ K}^{-1}$

and is considered as insignificant, according to the student's *t* test.

How future SATs change as the gSATs increase is discussed using Fig. 6. Here, Tmean, Tmax, and Tmin are the averages for all grid points located over the Japanese Islands. The Tmean increases are 1.2 K, 1.9 K, and 4.6 K for the d1.5, d2, and d4 cases, respectively, relative to those of PAST. Namely, they are approximately linearly 1.3 times larger than the gSAT increases. Therefore, it is concluded that future changes in the Tmean values are generally scalable with respect to global warming levels. Similarly, the Tmax and Tmin increases are scalable with factors of 1.2 and 1.6 to the gSAT, respectively. Due to reductions of snow coverage, the Tmin rate of increase is higher than that of the Tmean. Since the Tmean is approximately average of the Tmax and the

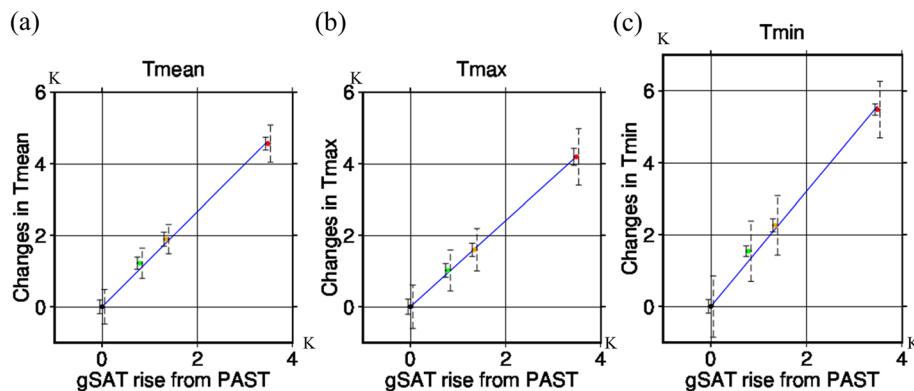


Fig. 6 Future changes in Tmean, Tmax, and Tmin. **a** Tmean, **b** Tmax, and **c** Tmin are averaged on all land grids on the Japanese Islands relative to those of PAST as a function of gSAT increases. The bars with solid line indicate standard errors of the ensemble mean, and the bars with dashed line indicate standard deviations. Linearly fitted line is shown in each panel. The black, green, yellow, and red circles indicate PAST, d1.5, d2, and d4, respectively

Tmin, the increase rate of the Tmean is larger than that of the Tmax. The standard errors of ensemble-mean temperatures are small, and therefore, the future changes in the mean value of the Tmean, Tmax, and Tmin are regarded to be significant. The standard deviations of the Tmean are smaller than that of the Tmax and Tmin. The spread of the Tmean, Tmax, and Tmin has no apparent response to the gSAT rises. Since the SAT in the Japanese Islands rises linearly, assuming 3 K rise in gSAT, Tmean, Tmax, and Tmin is estimated to be 3.2 K, 2.9 K, and 3.9 K, respectively.

Future changes in precipitation

Figure 7 shows 3 month accumulated precipitation amounts and the average SLP. In winter, d1.5, d2, and d4 all show trend patterns of the changes in the SLP similar to those seen in previous studies (Kimoto 2005, Hori and Ueda 2006, and Kawase et al. 2015): low SLPs in the west and high SLPs in the east. It is thought that the continental SLPs become lower because the temperature increases are greater on the Eurasian continent than for the oceans (Fig. 4).

Commonly, in d1.5, d2, and d4, future summer precipitation levels tend to decrease around Honshu and to increase outside of this area (Fig. 7e–h). Winter precipitation tends to increase over the Sea of Japan and to decrease south of the Japanese Islands, while the Sea of Japan side of Honshu shows decreases in winter precipitation (Fig. 7a–d).

Here, we define the SLP difference between two grid points, (130°E, 37°N) and (140°E, 37°N) as an index of the strength of the characteristic atmospheric SLP distribution in winter, i.e., high SLPs in the west and low SLPs in the east. Large indices are reflected by stronger winter monsoons, and the pattern is opposite to that of the future changes mentioned above. The index is 3.98 hPa in PAST and decreases by 0.16 hPa, 0.26 hPa, and 0.47 hPa in d1.5, d2, and d4, respectively. The changes in the indices are closely scalable with respect to gSAT increases. In summer, the SLPs south of Japan become higher and the SLPs east of Japan become lower in d1.5, d2, and d4 (Fig. 7). The subtropical high pressure zone, which covers the Japanese Islands in summer, retreats in the east of Japan and extends to the areas south of Japan in the future climate compared to the present climate. The changes in SLPs in the rectangular region from 27°N to 38°N and from 145°E to 152°E are -0.19 , -0.29 , and -0.78 hPa in d1.5, d2, and d4, respectively, and these are mostly scalable. Those in the area from 24°N to 26°N and from 125°E to 135°E are also scalable: $+0.25$, $+0.31$, and $+0.70$ hPa for d1.5, d2, and d4, respectively. In summary, the SLP changes in winter and summer appear as scalable changes to global warming.

Table 3 shows the correlation coefficient patterns of precipitation changes in the Japanese Islands. The correlation coefficients for the changes in annual and seasonal average precipitation amounts between future climate experiments are very high. This indicates that the changes in precipitation amounts appear similarly regardless of the temperature increase, thus responding to the future SST trend patterns prescribed. In JJA, the changes in precipitation amounts are highly correlated between d1.5 and d2. In contrast, there are lower correlation coefficients between d1.5 and d4 and between d2 and d4 than for the other cases. As presented later, these are unlikely to respond simply to future SLP changes (Fig. 7).

One of the characteristics of the Japanese climate is the seasonal contrast of precipitation events on the Sea of Japan side and on the Pacific Ocean side, which are separated by the central mountains. Figure 8 shows the future changes of precipitation amounts on the two sides of Honshu.

In winter, dry climate states generally appear on the Pacific Ocean side in the present climate conditions, but the precipitation amounts increase in the future (red squares in Fig. 8). By contrast, precipitation events, including snowfall, decrease on the Sea of Japan side (blue squares). These future tendencies are statistically significant and scalable. The possible reasons are as follows. Because the southeasterly winds from the Pacific Ocean to the Japanese Islands become stronger due to future changes in the circulation field in winter, precipitation amounts increase in the areas on the Pacific side, located on the windward side of the mountains. Conversely, precipitation decreases on the Sea of Japan side, where the northwesterly winds from the Sea of Japan become weaker.

On the other hand, in summer, there is a large jump between d4 and the other cases. The areas of Honshu with reduced precipitation become wider in d4 than in the other two experiments. Concurrently, in d4, the subtropical high around Okinawa is stronger than in d1.5 and d2, and extends to around Kyushu (Fig. 7f–h) and weakens east of Japan. As a result, the surface wind changes show divergence around Honshu due to both the strengthening of the southwesterly winds on the Sea of Japan side and the strengthening of northerly winds on the Pacific Ocean side. Therefore, summer precipitation amounts decrease on both the Sea of Japan side and on the Pacific side in Honshu (Fig. 8). However, Ose (2019) pointed out that future changes in summer precipitation around Japan are highly uncertain although the decrease in summer precipitation around Japan is predicted by several models.

Although future precipitation changes vary depending on seasons and regions, the annual precipitation

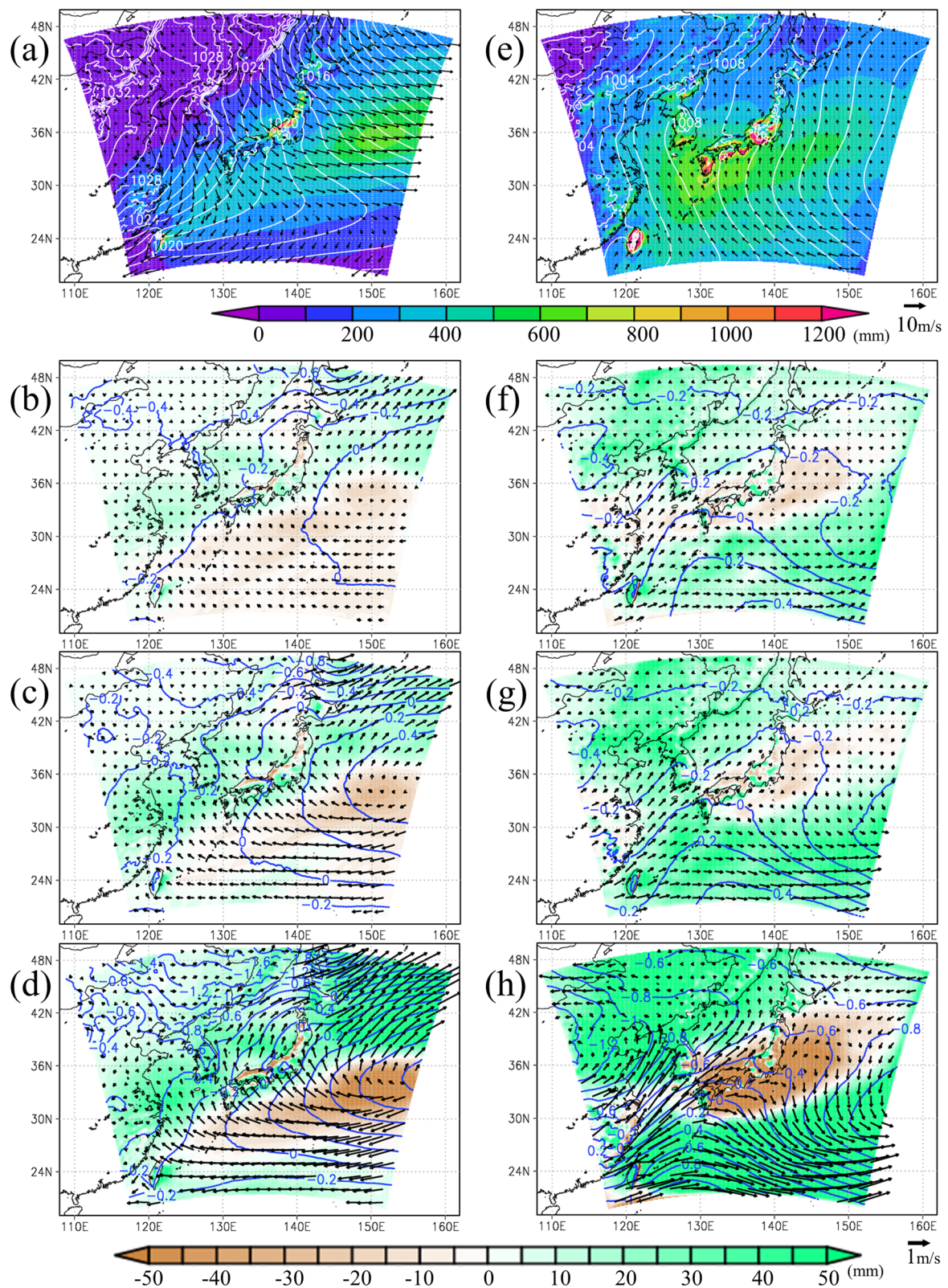


Fig. 7 Seasonal precipitation amounts and seasonal average SLPs and wind vectors. The shading, contours, and vectors denote precipitation amounts (mm), SLPs (hpa), and wind vectors (ms^{-1}), respectively, for (a, b, c, and d) DJF and (e, f, g, and h) JJA. a and e show the climatologies of PAST and the future changes of (b and f) d1.5, (c and g) d2, and (d and h) d4 are presented

Table 3 Pattern correlation coefficients of future changes in precipitation amounts

	d1.5 vs d2	d1.5 vs d4	d2 vs d4
ANNUAL	0.94	0.88	0.94
DJF	0.96	0.92	0.96
MAM	0.94	0.95	0.95
JJA	0.91	0.59	0.64
SON	0.90	0.95	0.89

The values are the pattern correlation coefficients of future changes in annual and seasonal precipitation amounts for all grid points in the Japanese Islands between two selected levels of warming

amounts in Japan have no clear relationship with gSAT increases (Fig. 9a). The future precipitation changes of d4 seen largely in Fig. 8 are mostly canceled out. The future annual precipitation amounts appear to significantly increase in the future climate simulations by approximately 0.8%. Whereas the increases in mean value of annual precipitation due to moisture increase with the gSAT rises are canceled out by changes in circulation fields, the standard deviations of annual precipitation become large because of the moisture increase

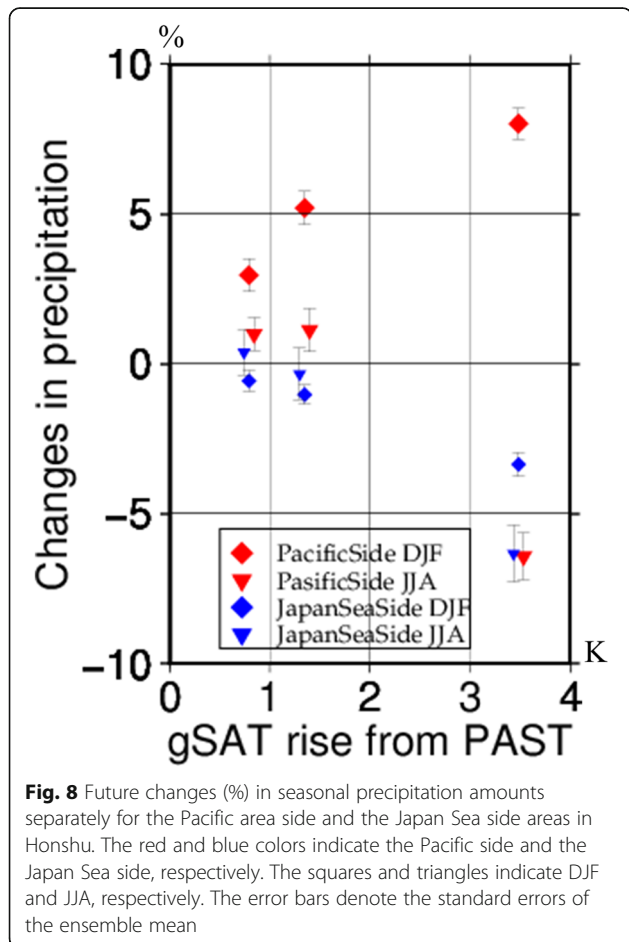


Fig. 8 Future changes (%) in seasonal precipitation amounts separately for the Pacific area side and the Japan Sea side areas in Honshu. The red and blue colors indicate the Pacific side and the Japan Sea side, respectively. The squares and triangles indicate DJF and JJA, respectively. The error bars denote the standard errors of the ensemble mean

(Pendergrass et al. 2017). The future R1d values increase approximately linearly with the global warming levels (Fig. 9b), and the increase rates are $7\% K^{-1}$, $6\% K^{-1}$, and $5\% K^{-1}$ at d1.5, d2, and d4 respectively. These values agree with the theoretical values from the Clausius-Clapeyron (CC) relationship of 6 to $7\% K^{-1}$ for strong precipitation (e.g., Wang et al. 2017; Gao et al. 2018). The increase rates of R1d become slightly smaller as the gSAT rises due to the development of the divergence fields in summer (Fig. 7). The standard errors of ensemble-mean R1d indicate that the increase of R1d due to global warming is regarded to be significant. The standard deviations of R1d become large as the gSAT rises and this result is caused by moisture increases and occurrence frequency increases in intense tropical cyclones in the future climate (Yoshida et al. 2017; Kitoh and Endo 2019).

Impacts of a 0.5° increase on regional climates

By implementing additional mitigation measures which limit the gSAT rise by + 1.5 K, it is expected that the Tmean increases over Japan would be reduced by 0.7 K (Fig. 6) compared to those of the present climate. As shown in Fig. 5, the north-south contrast in SAT increases is small in d1.5, while it becomes larger in d2 and d4. The impact of a 0.5 K rise from d1.5 in the gSAT on the summer temperatures in Japan is 0.85 K in the north and 0.51 K in the south. Similarly, the R1d precipitation amounts over the Japanese Islands increase significantly between + 1.5 and + 2 K (Fig. 9). Changes in the circulation fields cause a significant increase in winter precipitation on the Pacific side of 2.5% (Fig. 8), while the winter precipitation amounts on the Sea of Japan side do not exhibit a significant difference between + 1.5 and + 2 K.

The increase in R1d due to gSAT rise of 0.5 K is about $4.0\% K^{-1}$ on average for all land grids on the Japanese Islands, which is smaller than the theoretical value of 6 to $7\% K^{-1}$. There are regional characteristics in the differences in R1d, and it is small at latitudes from $34^{\circ}N$ to $41^{\circ}N$ (Fig. 10). The differences of R1d in Hokkaido, located north of $41^{\circ}N$, are larger than other regions due to larger increases in the SATs and close to the theoretical value (Table 4). In Kyushu, located south of $34^{\circ}N$, the increase rate of R1d, within the standard error range, does not deviate from the theoretical value. In contrast, the increase rate of R1d in Honshu is significantly smaller than the theoretical value because the divergence tendency with the progression of global warming prevents increase in R1d (Fig. 7).

Conclusions

In this study, we confirmed the reproducibility seen in the regional climate model outputs of the d4PDF and

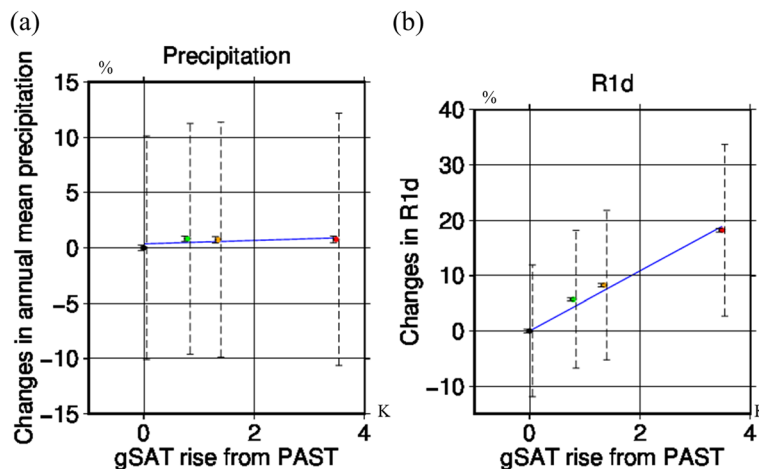


Fig. 9 Changes in annual mean precipitation and R1d. Changes in **a** annual mean precipitation relative to the gSAT increases and in **b** R1d relative to the gSAT increases. Values are averaged on all land grids on the Japanese Islands. The solid bars indicate standard errors of the ensemble mean, and the dashed bars indicate standard deviations. The blue color denotes linear fitting. The black circle, green circle, yellow circle, and red circle indicate PAST, d1.5, d2, and d4, respectively

investigated the scalability of future changes in SATs, SLPs, and precipitation amounts. The present climate reproducibility of the regional climate model in the d4PDF was confirmed, and it was found that the NHRCM20 performs reasonably comparably to the higher-resolution models for SATs and precipitation at daily time scales.

As a subset of the d4PDF, future climate simulations of the + 1.5 K gSATs were performed. The scalability, that is, the linearity of future changes with gSAT

increases, was examined by comparing with the PAST, d2, and d4 (already available) cases. The future SAT changes in Japan showed a scalable relationship with respect to the gSAT increases for faster rates of warming than that of the gSAT. The meridional warming contrast of the SATs is enhanced as global warming becomes severe. In winter, the zonal SLP differences over Japan decrease, while in summer, the SLPs increase (decrease) south (east) of Japan. These future SLP changes in winter and summer are scalable and weaken the seasonal monsoons. The average precipitation amounts are mostly unchanged regardless of the gSAT increases. Winter precipitation amounts on the Pacific side of the Japanese Islands increase linearly with gSAT increases, while those on the Sea of Japan side decrease linearly. The changes of summer precipitation are not scalable because the areal expansion of the divergence of surface winds around Japan reduces precipitation. Future changes in heavy daily precipitation amounts are scalable to gSAT increases, showing rates of 5–7% K⁻¹. If the gSAT increase is reduced from + 2 to + 1.5 K by implementing mitigation measures, the Tmean rise in Japan would be reduced by 0.7 K. Heavy precipitation would also be decreased by 2.7% over the Japanese Island. The

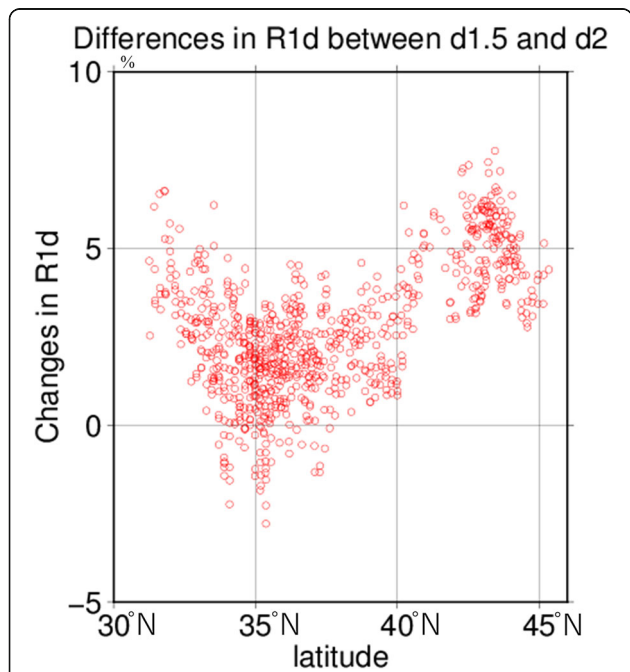


Fig. 10 Differences in R1d (%) between d1.5 and d2 on land grids in the Japanese Islands

Table 4 Differences in R1d (dR1d) and SAT (dSAT) between d1.5 and d2 with standard errors of the ensemble mean

	dR1d(%)	dSAT(K)	dR1d/dSAT(%K ⁻¹)
ALL	2.7 ± 0.4	0.67 ± 0.28	4.0 ± 1.1
Hokkaido	5.0 ± 0.8	0.74 ± 0.26	6.8 ± 1.3
Kyushu	3.3 ± 0.8	0.62 ± 0.26	5.3 ± 1.1
Honshu	2.0 ± 0.5	0.65 ± 0.27	3.1 ± 0.5

The right column shows the increase rate of the R1d per 1 K (dR1d/dSAT). All land grids in the Japanese Islands are used for ALL

increase rate of heavy precipitation has regional characteristics. In Hokkaido, where the SAT warming is the greatest in Japan, the increase rate is larger than other regions, and in Honshu, where SLP have divergent tendency under the global warming conditions, the increase rate is smaller than other regions.

Downscale experiments with fine-resolution models are useful for discussing detailed terrain effects on future climate states. To deal with a wide range of uncertainties in future predictions, ensemble experiments using various regional climate models and ocean-coupled simulations are required. In addition, performing experiments using different levels of global warming will help to elucidate those phenomena that are not scalable. All of these will be future works.

Supplementary information

Supplementary information accompanies this paper at <https://doi.org/10.1186/s40645-020-00341-3>.

Additional file 1: Figure S1. The distribution of Δ SST in DJF and JJA averaged for all ensemble members. The first row (a, b, and c) shows the distributions in JJA and second row (d, e, and f) shows the distributions in DJF. The future changes of d1.5, d2, and d4 are presented in the left (a and d), center (b and e), and right (c and f) columns, respectively.

Abbreviations

CCSM4: Community Climate System Model version 4; CMIP5: Coupled Model Intercomparison Project Phase 5; d4PDF: Database for Policy Decision making for future climate change; GFDL-CM3: Geophysical Fluid Dynamics Laboratory; HadGEM2-AO: Hadley Centre Global Environmental Model version 2 AO; MIROC5: Model for Interdisciplinary Research on Climate version 5; MPI-ESM-MR: Max Planck Institute for Meteorology Earth System Model MR; MRI-AGCM: Meteorological Research Institute Atmospheric General Circulation Model; MRI-CGCM: Meteorological Research Institute Coupled Atmosphere-Ocean General Circulation Model; NHRM: Non-Hydrostatic Regional Climate Model; RCP8.5: Representative Concentration Pathway with a radiative forcing level of 8.5 Wm^{-2} ; CC: Clausius-Clapeyron

Acknowledgments

This work was conducted under the SOUSEI and TOUGOU Programs of the Japan MEXT.

Authors' contributions

MN, MI, and HS proposed the topic. MN carried out the experiments, analyzed the data and drafted the manuscript. MI provided SST data and sea ice distribution data. HS provides the scaling factors. RM supported the numerical design environment. MI, RM, AM, HK, and HS discussed the analyses and the results. All of the authors read and approved the final manuscript.

Funding

This work was conducted under the SOUSEI and TOUGOU Programs of the Ministry of Education, Culture, Sports, Science, and Technology (MEXT) of Japan.

Availability of data and materials

The experiments under the present climate conditions, + 2 K, and + 4 K of the d4PDF data set are available from the DIAS website (<http://www.diasjp.net/en/>), and the experiment under + 1.5 K climate conditions will be available from the DIAS website.

Competing interests

The authors declare that they have no competing interests.

Author details

¹Meteorological Research Institute, 1-1 Nagamine, Tsukuba, Ibaraki 305-0052, Japan. ²National Institute for Environmental Studies, 16-2 Onogawa, Tsukuba, Ibaraki 305-8506, Japan.

Received: 25 December 2019 Accepted: 22 May 2020

Published online: 23 June 2020

References

- Fujita M, Mizuta R, Ishii M, Endo H, Sato T, Okada Y, Kawazoe S, Sugimoto S, Ishihara K, Watanabe S (2019) Precipitation changes in a climate with 2-K surface warming from large ensemble simulations using 60-km global and 20-km regional atmospheric models. *Geophys Res Lett* 45. <https://doi.org/10.1029/2018GL079885>
- Gao X, Zhu Q, Yang Z, Liu J, Wang H, Shao W, Huang G (2018) Temperature dependence of hourly, daily, and event-based precipitation extremes over China. *Sci Rep* 8:17564. <https://doi.org/10.1038/s41598-018-35405-4>
- Hirahara S, Ishii M, Fukuda Y (2014) Centennial-scale sea surface temperature analysis and its uncertainty. *J Clim* 27:57–75. <https://doi.org/10.1175/JCLI-D-12-00837.1>
- Kawase H, Sasaki H, Murata A, Nosaka M, Ishizaki NN (2015) Future changes in winter precipitation around Japan projected by ensemble experiments using NHRM. *J Meteorol Soc Jpn* 93:571–580. <https://doi.org/10.2151/jmsj.2015-034>
- Kawase H, Murata A, Mizuta R, Sasaki H, Nosaka M, Takayabu I (2016) Enhancement of heavy daily snowfall in central Japan due to global warming as projected by large ensemble of regional climate simulations. *Clim Chang* 139:265–278. <https://doi.org/10.1007/s10584-016-1781-3>
- Kitoh A, Endo H (2019) Future changes in precipitation extremes associated with tropical cyclones projected by large-ensemble simulations. *J Meteorol Soc Japan* 97:141–152
- Leduc M, Mailhot A, Frigon A, Martel J-L, Ludwig R, Brietzke GB, Giguère M, Brissette F, Turcotte R, Braun M, Scinocca J (2019) ClimEx project: a 50-member ensemble of climate change projections at 12-km resolution over Europe and northeastern North America with the Canadian Regional Climate Model (CRCM5). *J Appl Meteorol Climatol* 58:663–693. <https://doi.org/10.1175/jamc-d-18-0021.1>
- Lee, D., S. K. Min, E. Fischer, H. Shiogama, I. Bethke, L. Lierhammer and J. F. Scinocca, 2018: Impacts of half a degree additional warming on the Asian summer monsoon rainfall characteristics. *Environ Res Lett* 13. doi:<https://doi.org/10.1088/1748-9326/aab55d>, 044033.
- Liu W, Sun F, Lim WH, Zhang J, Wang H, Shiogama H, Zhang Y (2018) Global drought and severe drought-affected populations in 1.5 and 2 °C warmer worlds. *Earth Syst Dynam* 9:267–283. <https://doi.org/10.5194/esd-9-267-2018>
- Masson-Delmotte, V., P. Zhai, H.-O. Pörtner, D. Roberts, J. Skea, P.R. Shukla, A. Pirani, W. Moufouma-Okia, C. Péan, R. Pidcock, S. Connors, J.B.R. Matthews, Y. Chen, X. Zhou, M.I. Gomis, E. Lonnoy, T. Maycock, M. Tignor, and T. Waterfield, (Eds.) 2018: IPCC global warming of 1.5 °C, World Meteorological Organization.
- Matsumura S, Sato T (2011) Snow/ice and cloud responses to future climate change around Hokkaido. *Sola* 7:205–208. <https://doi.org/10.2151/sola.2011-052>
- Mitchell D, James R, Forster P, Betts R, Shiogama H, Allen M (2016) Realizing the impacts of a 1.5 °C warmer world. *Nat Clim Chang* 6:735–737. <https://doi.org/10.1038/nclimate3055>
- Mitchell D, AchutaRao K, Allen M, Bethke I, Beyerle U, Ciavarella A, Forster PM, Fuglestedt J, Gillett N, Haustein K, Ingram W, Iversen T, Kharin V, Klingaman N, Massey N, Fischer E, Schleussner CF, Scinocca J, Seland Ø, Shiogama H, Shuckburgh E, Sparrow S, Stone D, Uhe P, Wallom D, Wehner M, Zaaboul R (2017) Half a degree additional warming, prognosis and projected impacts (HAPPI): background and experimental design. *Geosci Model Dev* 10:571–583. <https://doi.org/10.5194/gmd-10-571-2017>
- Mizuta R, Yoshimura H, Murakami H, Matsueda M, Endo H, Ose T, Kamiguchi K, Hosaka M, Sugi M, Yukimoto S, Kusunoki S, Kitoh A (2012) Climate simulations using the improved MRIAGCM with 20-km grid. *J Meteorol Soc Jpn* 90A:233–258. <https://doi.org/10.2151/jmsj.2012-A12>
- Mizuta R, Murata A, Ishii M, Shiogama H, Hibino K, Mori N, Arakawa O, Imada Y, Yoshida K, Aoyagi T, Kawase H, Mori M, Okada Y, Shimura T, Nagatomo T, Ikeda M, Endo H, Nosaka M, Arai M, Takahashi C, Tanaka K, Takemi T, Tachikawa Y, Temur K, Kamae Y, Watanabe M, Sasaki H, Kitoh A, Takayabu I, Nakakita E, Kimoto M (2017) Over 5000 years of ensemble future climate simulations by 60 km global and 20 km regional atmospheric models. *Bull Amer Meteorol Soc* 98:1383–1398. <https://doi.org/10.1175/BAMS-D-16-0099.1>

- Murata A, Sasaki H, Kawase H, Nosaka M, Aoyagi T, Ohizumi M, Seino N, Shido F, Hibino K, Ishihara K, Murai H, Yasui S, Wakamatsu S, Takayabu I (2017) Projection of future climate change over Japan in ensemble simulations using a convection-permitting regional climate model with urban canopy. *Sola* 13:219–223. <https://doi.org/10.2151/sola.2017-040>
- Ose T (2019) Characteristics of future changes in summertime East Asian monthly precipitation in MRI-AGCM global warming experiments. *J Meteorol Soc Jpn* 97:317–335. <https://doi.org/10.2151/jmsj.2019-018>
- Pendergrass AG, Knutti R, Lehner F et al (2017) Precipitation variability increases in a warmer climate. *Sci Rep* 7:17966 <https://doi.org/10.1038/s41598-017-17966-y>
- Sasaki H, Kurihara K, Takayabu I, Uchiyama T (2008) Preliminary experiments of reproducing the present climate using the non-hydrostatic regional climate model. *Sola* 4:25–28. <https://doi.org/10.2151/sola.2008-007>
- Sasaki H, Murata A, Hanafusa M, Ohizumi M, Kurihara K (2011) Reproducibility of present climate in a non-hydrostatic regional climate model nested within an atmosphere general circulation model. *SOLA* 7:173–176. <https://doi.org/10.2151/sola.2011-044>
- Scherrer SC, Ceppi P, Croci-Maspoli M, Appenzeller C (2012) Snow-albedo feedback and Swiss spring temperature trends. *Theor Appl Climatol* 110:509–516. <https://doi.org/10.1007/s00704-012-0712-0>
- Shiogama H, Hasegawa T, Fujimori S, Murakami D, Takahashi K, Tanaka K, Emori S, Kubota I, Abe M, Imada Y, Watanabe M, Mitchell D, Schaller N, Sillmann J, Fischer EM, Scinocca JF, Bethke I, Lierhammer L, Takakura J, Trautmann T, Döll P, Ostberg S, Schmied HM, Saeed F, Schleussner CF (2019) Limiting global warming to 1.5 °C will lower increases in inequalities of four hazard indicators of climate change. *Environ Res Lett* 14. <https://doi.org/10.1088/1748-9326/ab5256> 124022
- Takayabu I, Hibino K (2016) The skillful time scale of climate models. *J Meteorol Soc Jpn* 94A:191–197. <https://doi.org/10.2151/jmsj.2015-038>
- von Trentini F, Leduc M, Ludwig R (2019) Assessing natural variability in RCM signals: comparison of a multi model euro-CORDEX ensemble with a 50-member single model large ensemble. *Clim Dyn* 53:1963–1979. <https://doi.org/10.1007/s00382-019-04755-8>
- Wang G, Wang D, Trenberth KE, Erfanian A, Yu M, Bosilovich M, Parr DT (2017) The peak structure and future changes of the relationships between extreme precipitation and temperature. *Nat Clim Chang* 7:268–274. <https://doi.org/10.1038/nclimate3239>
- Yoshida K, Sugi M, Mizuta R, Murakami H, Ishii M (2017) Future changes in tropical cyclone activity in high-resolution large-ensemble simulations. *Geophys Res Lett* 44:9910–9917

Publisher's Note

Springer Nature remains neutral with regard to jurisdictional claims in published maps and institutional affiliations.

Submit your manuscript to a SpringerOpen[®] journal and benefit from:

- Convenient online submission
- Rigorous peer review
- Open access: articles freely available online
- High visibility within the field
- Retaining the copyright to your article

Submit your next manuscript at ► [springeropen.com](https://www.springeropen.com)
